Mu and epsilon near zero metamaterials for perfect coherence and new antenna designs

Jing Jing Yang[1], Yan Francescato[1,2], Stefan A Maier[2], Fuchun Mao[1], Ming Huang[1, a]

[1] *Wireless Innovation Lab of Yunnan University, Kunming 65009, China*
[2] *The Blackett Laboratory, Imperial College London, London SW7 2AZ, United Kingdom*
[a] huangming@ynu.edu.cn

Abstract: Wave interference is a fundamental physical phenomenon. Traditionally, the coherent effect of two identical point sources only takes place when the optical path is an integer number of wavelengths. In this paper, we show that mu and epsilon near zero (MENZ) metamaterials can be used to realize a perfectly constructive and isotropic interference. No matter how many point sources are embedded in the MENZ region, the wavefronts overlap perfectly. This translates into a total relaxation of the conventional condition for coherence enabled by the apparent infinite wavelength of the fields within MENZ metamaterials. Furthermore, we investigate crucial parameters such as the shape and size of the MENZ region. We demonstrate that flat sided geometries give rise to constructive interference beams serving as a powerful design mean. We also reveal the importance of relying on deeply sub-wavelength MENZ volumes as larger sizes increase the impedance and therefore reduce the output power of the device. The proposed concepts bear significance for current trends in antenna design which are inspired by the recent developments of electromagnetic metamaterials. Moreover, the perfect coherence effect can be appealing for power combiners, especially in the terahertz where sources are dim, as the irradiation intensity scales with the square of the number of embedded sources.

OCIS codes: (260.3160) Interference; (160.3918) Metamaterials; (070.7345) Wave propagation.

References and links

1. H. D Lee,E. J. Jung, M. Y. Jeong, Z. Chen and C. S. Kim, "Uniform spacing interrogation of a Fourier domain mode-locked fiber Bragg grating sensor system using a polarization-maintaining fiber Sagnac interferometer," Measurement Science and Technology **24**(6), 065101 (2013).
2. W. Yuan, L. Khan,D. J. Webb, K. Kalli, H. K. Rasmussen, A. Stefani, and O. Bang, "Humidity insensitive TOPAS polymer fiber Bragg grating sensor," Optics Express **19**(20), 19731-19739 (2011).
3. X. Fang, C. R. Liao, and D. N. Wang, "Femtosecond laser fabricated fiber Bragg grating in microfiber for refractive index sensing," Optics letter **35**(7), 1007-1009 (2010).
4. H. Müller, A. Peters, and S. Chu, "A precision measurement of the gravitational redshift by the interference of matter waves," Nature **463**(7283), 926-929 (2009).
5. R. Ishikawa, E. Okunishi, H. Sawada, Y. Kondo, F. Hosokawa, and E. Abe, "Direct imaging of hydrogen-atom columns in a crystal by annular bright-field electron microscopy," Nature materials **10**(4), 278-281 (2011).
6. J. J. Li, X. F. Zang, J. F. Mao, M. Tang, Y. M. Zhu, S. L. Zhuang, "Overlapped optics induced perfect coherent effects," Scientific Reports **3**, 3569 (2013).
7. X. F. Zang, C. Shi, Z. Li, L. Chen, B. Cai, Y. M. Zhu, H. B. Zhu, "Illusion induced overlapped optics," Optics Express **22**(1), 582-592 (2014).
8. J. B. Pendry, D. Schurig, and D. R. Smith, "Controlling electromagnetic fields," Science **312**(5781), 1780 (2006).
9. U. Leonhardt, "Optical conformal mapping," Science **312**(5781), 1777 (2006).
10. J. B. Pendry, A. I. Fernández-Domínguez, Yu Luo, and R.Zhao, "Capturing photons with transformation optics," Nature Physics **9**(8), 518-522 (2013).
11. R. Zhao, Y. Luo, A. I. Fernández-Domínguez, and J. B. Pendry, "Description of van der Waals Interactions Using Transformation Optics," Phys. Rev. Lett. **111**(3), 033602 (2013).

12. J. J. Yang, M. Huang, C. F. Yang, Z. Xiao, and J. H. Peng, "Metamaterial electromagnetic concentrators with arbitrary geometries," Optics Express **17**(22), 19656-19661 (2009).
13. T. H. Li, M. Huang, J.J. Yang, W. J. Zhu, and J. Zeng, "A Novel Method for Designing Electromagnetic Shrinking Device with Homogeneous Material Parameters," IEEE Transaction on Magnetics **49**(10), 5280-5286 (2013).
14. K. Zhang, Q. Wu, F.-Y. Meng, and L.-W. Li, "Metamaterials With Tunable Negative Permeability Based on Mie Resonance," IEEE Transactions on Magnetics **48**(11), 4289-4292 (2012).
15. H. Y. Chen, and C. T. Chan, "Acoustic cloaking and transformation acoustics," J. Phys. D: Appl. Phys. **43**(11), 113001 (2010).
16. J. J. Yang, M. Huang, G. H. Cai, R. S. Xie, and J. Yang, "Design of Acoustic Metamaterial Devices Based on Inverse Method," J. Vib. Acoust. **135**(5), 051024 (2013).
17. S. Guenneau, C. Amra, and D. Veynante, "Transformation thermodynamics: cloaking and concentrating heat flux," Optics Express **20**(7), 8207-8218 (2012).
18. R. Schittny, M. Kadic1, S. Guenneau, and M.Wegener, "Experiments on Transformation Thermodynamics: Molding the Flow of Heat," Phys. Rev. Lett. **110**(19), 195901(2013).
19. A. Alù, M. G. Silveirinha, A. Salandrino, and N. Engheta, "Epsilon-near-zero metamaterials and electromagnetic sources: Tailoring the radiation phase pattern," Phys. Rev. B. **75**(15), 155410 (2007).
20. A. A. Basharin, C. Mavidis, M. Kafesaki, E. N. Economou, and C. M. Soukoulis, "Epsilon near zero based phenomena in metamaterials," Phys. Rev. B **87**(15), 155130 (2013).
21. A. Ourir, A. Maurel, and V. Pagneux, "Tunneling of electromagnetic energy in multiple connected leads using ϵ-near-zero materials," Optics Letters **38**(2), 2092 (2013).
22. R. W. Ziolkowski, "Propagation in and scattering from a matched metamaterial having a zero index of refraction," Phys. Rev. E **70**(4), 046608 (2004).
23. W. Zhu, I. D. Rukhlenko, and M. Premaratne, "Application of zero-index metamaterials for surface plasmon guiding, " Appl. Phys. Lett. 102(1), 011910 (2013).
24. J. J. Yang, M. Huang, and J. H. Peng, "Directive Emission Obtained by Mu and Epsilon-Near-Zero Metamaterials," Radioengineering **18**(2), 124-128 (2009).
25. B. Wang, and K. M. Huang, "Shaping the radiation pattern with Mu and Epsilon-near-zero metamaterials," Progress In Electromagnetics Research **106**, 107-119 (2010).
26. Q. Cheng, W. X. Jiang,and T. J. Cui, "Multi-beam generations at pre-designed directions based on anisotropic zero-index metamaterials," Appl. Phys. Lett., **99**(13), 131913 (2011).
27. H. Suchowski, K. O'Brien, Z. J. Wong, A. Salandrino, X. Yin, and X. Zhang, "Phase Mismatch–Free Nonlinear Propagation in Optical Zero-Index Materials," Science **342**(6163), 1223 (2013).
28. Q. Cheng, W. X. Jiang,and T. J. Cui, "Spatial Power Combination for Omnidirectional Radiation via Anisotropic Metamaterials, " Phys. Rev. Lett., 108(21), 213903 (2012).
29. M. Silveirinha, and N. Engheta, "Design of matched zero-index metamaterials using nonmagnetic inclusions in epsilon-near-zero media," Phys. Rev. B **75**(7), 075119 (2007).

1. Introduction

Historically, coherent effects have helped confirm the wave nature of light and electrons. The interference of waves is one of the most important and useful phenomena in modern physics. For example, the effects of the mode transformation, band gap formation and diffraction compensation observed in Bragg structures, which have been widely used in sensing applications [1-3] are due to resonant constructive interferences of waves scattered on periodic perturbations which take place in the vicinity of the Bragg resonance. It has also been shown that the quantum interference of atoms will give rise to a precision measurement of the gravitational redshift [4], and the coherent effect is the key factor in enhancing the resolution of imaging systems [5]. In the traditional coherent effect picture, two separated identical point sources can interfere perfectly with each other only when the optical path difference is an integer number of wavelengths, which leads to alternating dark and bright fringes for different optical path difference. Such a perfect coherent condition seemed insurmountable. However, recently, it has been demonstrated that based on transformation optics, two separated in-phase identical point sources can induce perfect constructive interference with each other without satisfying the conventional coherent condition[6]. Furthermore, it was shown that invisibility cloaks can be applied to realize the overlapped optics [7], that is, multiple in-phase point sources located in the hidden region overlap each others, leading to a perfect optical coherent effect. The transformation optics firstly proposed by Pendry and Leonhardt [8, 9] in 2006 has provided us with a powerful paradigm for exploiting the potentials of optical metamaterials [10-14], and it has been extended to acoustics [15, 16] and thermal fields [17, 18] for

designing novel devices such as cloaks and concentrators. However, applications of the transformation optics technique usually lead to highly anisotropic and inhomogeneous solutions for the required permittivities and permeabilities of a device and are extremely difficult to implement in practice.

In the studies of metamaterials, a great attempt has been made to manipulate the behaviour of radiation waves to form a desired field distribution. Alù and his coworkers [19] studied the possibility of using epsilon-near-zero materials to tailor the phase pattern of the output radiation from an arbitrary source. Basharin et al. [20] then demonstrated that light transmission through dielectric cylinders embedded in an ENZ host can be strongly enhanced due to Mie resonances. Finally, Ourir et al. [21] showed that perfect electromagnetic energy transmission can be achieved by using ENZ material junctions. Based on mu and epsilon near zero (MENZ) metamaterials, also called zero-index materials (ZIM), which are impedance-matched to free space [22, 23], wavefront reshaping schemes were proposed [24-26] and phase matching-free devices and spatial power combination for omnidirectional radiation via anisotropic metamaterials demonstrated recently [27, 28]. In this paper, we prove that additionally to these effects, perfect coherence can be achieved using MENZ metamaterials. Thanks to their wavefront shaping ability we further show their use in the control of perfectly constructive beams and they could serve therefore as powerful mechanisms in future metamaterials-inspired antenna designs. Importantly, we report on the size effect of the MENZ region, as it is seen that at scales larger than a tenth of the operating wavelength an increase of the impedance reduces drastically the performance of the device. Last, we confirm our findings with an inductor-capacitor (L-C) transmission line medium approach. The circuit theory convincingly reproduces the perfect coherence effect and the size dependent efficiency.

2. Simulation results

2.1 Interferences between two sources

Generally, two or more separated waves can interfere with each other, when all of them have the same frequency, mode, and constant phase difference. Taking two in-phase point sources as an example, the total intensity I (in W/m^2) of the resulting interference wave can be written as

$$\mathrm{I}_{\mathrm{total}} = (\mathrm{I}_1 + \mathrm{I}_2)(1 + \frac{2\sqrt{\mathrm{I}_1\mathrm{I}_2}}{\mathrm{I}_1 + \mathrm{I}_2}\cos\delta), \quad (1)$$

where $\delta = k \times \Delta$, with $k = 2\pi / \lambda$ the wave vector of light and Δ the optical path difference between these two point sources. I_1 and I_2 are the corresponding intensity of each source. Assuming $\mathrm{I}_1 = \mathrm{I}_2 = \mathrm{I}_0$ yields:

$$\mathrm{I}_{\mathrm{total}} = 4\,\mathrm{I}_0 \cos^2(\frac{\pi\Delta}{\lambda}). \quad (2)$$

Obviously, it is seen that only when $\Delta = m\lambda$ will the total intensity of the two point sources be maximum and equal to $4\mathrm{I}_0$. This corresponds to the best coherent condition, at which the point sources overlap perfectly and are in phase with each other. The condition of perfect constructive coherence can be generalized to N sources where the maximum intensity is $\mathrm{N}^2\,\mathrm{I}_0$. If we now consider a MENZ region in which both the permittivity and permeability approach zero, the wavelength of electromagnetic waves propagating through the material tends to infinity. As a consequence, if the waves are initially in phase they will superpose perfectly at all points in space within the MENZ region creating an artificial new source with intensity $\mathrm{N}^2\,\mathrm{I}_0$. Note that if two waves are exactly out of phase they will cancel each other perfectly everywhere in space. When exiting the central region, the resulting superposition wave will therefore propagate as though it was originating from a single source. In case of a circular MENZ region, the radiation consists then of a spherical wave which does not exhibit

any interference pattern. In conclusion, the use of MENZ metamaterials makes it possible to realize perfect coherence without satisfying any particular interference condition. In what follows, numerical simulations are performed to verify this speculation and details of the MENZ metamaterial geometry are investigated.

2.2 Simulation model

We consider first a circular MENZ region with radius $R_1 = 0.025$ m placed in free space. The total computation domain ($R_2 = 0.4$ m) is truncated by perfectly matched layers (PML) of width $W = 0.07$ m in order to prevent wave reflections. The simulation model is shown in Fig.1 where the point dipoles are defined as line sources and embedded randomly in the MENZ region. The simulation is performed at the frequency of 6GHz (equivalent to a free-space wavelength of 0.05m) using the commercial finite-element (FEM) software COMSOL.

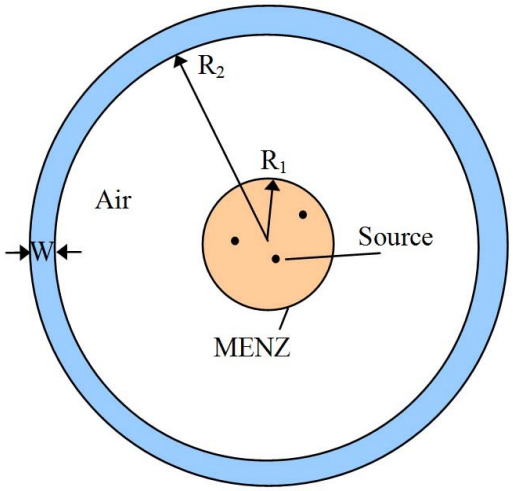

Fig.1. Simulation model showing the point sources, the MENZ region (in orange) and the PML region (in blue).

2.3. Perfect overlapped optics

Firstly, we simulate the wave interference phenomenon which arises between two identical point sources with an amplitude of 1A in free space. The distance between the two sources is 1.6λ. The resulting radiation pattern shown in Fig. 2(a) reveals an inhomogeneous field distribution characteristic of traditional wave coherence effects. Strikingly, when multiple point sources are embedded in the MENZ region the total field distribution becomes homogeneous, as shown in Fig. 2(b). The mechanism behind this phenomenon is that the phase front at the exit side of the MENZ metamaterials is conformed to the shape of the exit face since there is no phase variation in the wave propagation inside the material. Furthermore, the perfect coherent effect is independent of the position and the amount of point sources embedded in the MENZ region. We consider as an example N point sources, each one with an amplitude 1/N (A). The simulation results indicate that the far field intensity maps exactly that of a single dipole as we predicted, see Fig. 2(b) and (c). If we set the amplitude of each source to be 1(A), the far field power intensity of the simulation mode with N point sources can be increased by N^2 times, as illustrated in Fig.2(d). This could prove very helpful when available sources are excessively low power as in the terahertz regime.

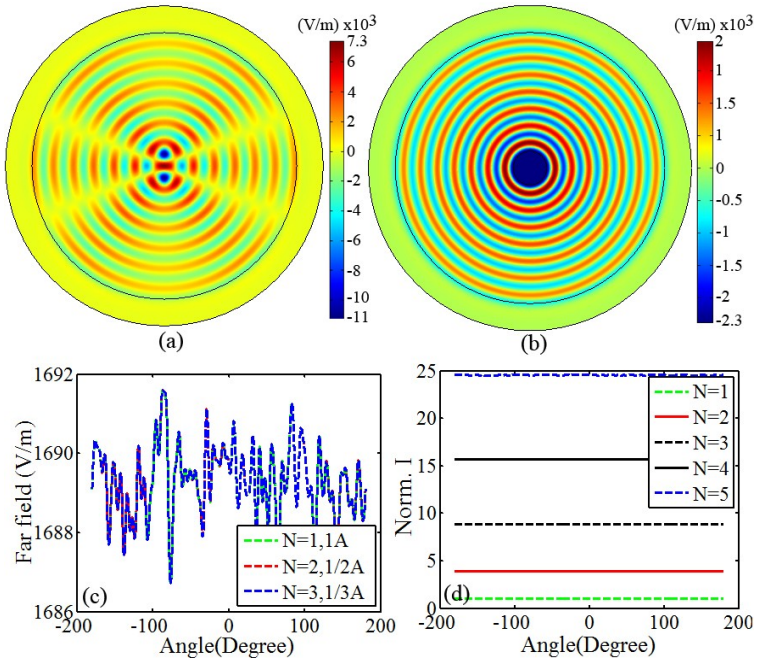

Fig.2. Electric field distribution in the computational domain. (a) Two identical in-phase point sources are located at the position of (0,-0.4m) and (0, 0.4m), respectively. (b) The two point sources are embedded in the MENZ region.(c) Far field for the structure with N point sources, each one has an intensity of 1/N (A). (d) Normalized far field power intensity for the structure with N point sources, each one has an intensity of 1(A).

2.4 Shape and size effect of the MENZ region

Interestingly, when we change the shape of the MENZ region to a square or a triangle, and place two point sources inside, the radiation will be divided into four and three beams, respectively, as shown in panels (a) and (b) of Fig. 3. Taking the four beam antenna as an example, the far field irradiation pattern is simulated and shown in Fig. 3(c). It is seen that due to the perfect coherent effects, increasing the number of the point source will enhance the intensity of the far field without affecting the radiation pattern. This provides powerful means for the designing of antennas with preferential scattering direction, where collimated beams will originate from the flat sides of the MENZ region. One can even choose to cover all the faces of that region but one with mirrors or opaque materials in order to achieve a single collimated beam with power $N^2 I_0$.

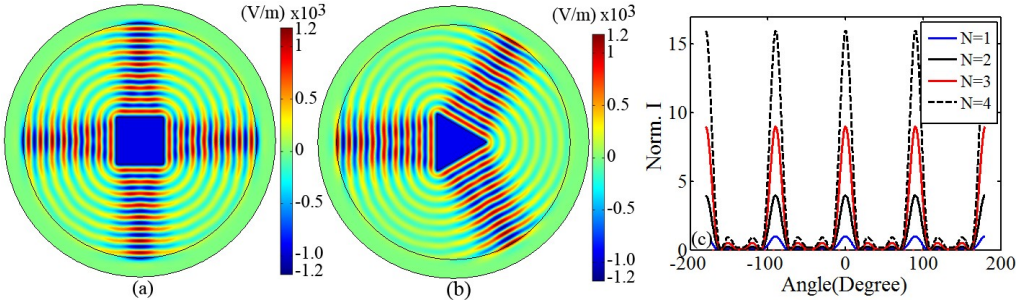

Fig.3. Electric field distribution of the computation domain with a square (a) and a triangle (b) MENZ region. (c) Normalized far field power intensity.

While to our knowledge there has been no discussion on the influence of the size of the MENZ region we observed a strong dependence of the scattered intensity, as shown by black symbols in Fig.4. There, the far-field power of a single point source is plotted as a function of the radius of the MENZ region normalized to the operating wavelength. As one can see, the output power follows an exponential decrease as the size of the central region increase and it saturates to its free-space value when the MENZ region is smaller than a tenth of the wavelength. Although there is no further detrimental effect due to the size, namely the radiation pattern and perfect coherence properties are conserved in all cases, this result sets an important criterion for the practical realization of MENZ-based devices. In order to verify this particular observation we plot as well the theoretical far-field power of a single source embedded in a circular MENZ region as first derived by Ziolkowski [22], see blue curve in Fig.4. The two results agree well but this is a rather surprising behaviour as MENZ metamaterials are expected to be impedance matched with free-space and they are assumed here as lossless. This actually stems from a "geometric impedance" as described by Silveirinha and Engheta [29]. Indeed even though the MENZ metamaterials has an impedance close to that of a vacuum, an additional impedance can be caused by a geometric mismatch. This is because the wavelength is near infinity in a MENZ region thus being effectively defined by the geometry itself. In the case of a waveguide with equal input and output cross-sections, this translates in a near unity transmission which is the "classical" MENZ scenario. Following Silveirinha and Engheta, a geometric reflection coefficient can be defined by the ratio $(L_i - L_o)/(L_i + L_o)$ where L_i is the point source effective size and L_O the external circumference of the MENZ region. This is plotted in Fig.4 as the red dashed line using $L_i = \lambda/80$. It is clear that an identical behaviour to our earlier results is recovered confirming the initial intuition.

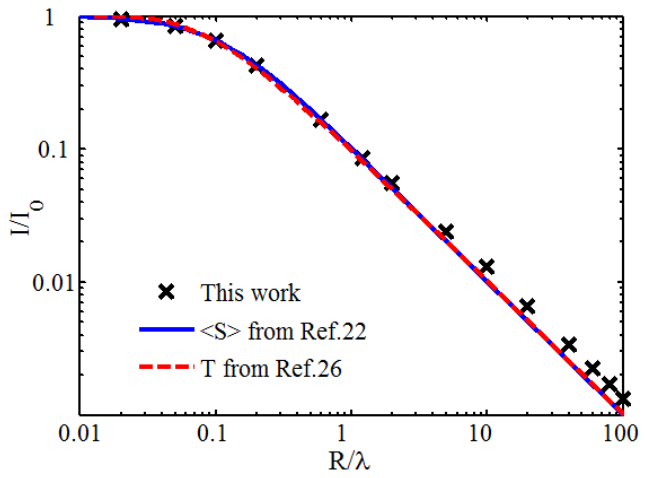

Fig.4. Far field power for a single point source embedded in a MENZ region with radius R/λ. Black crosses are for FEM simulations presented in this work, the blue line denotes the theoretical result as predicted by [22] and the interrupted red line represents the geometric transmission $T = 1 - |\rho|^2$ as derived in [29].

2.5 Demonstration based on LC network

Based on the well known circuit theory, we use an inductor-capacitor (LC) network to mimic the properties of MENZ metamaterials in this section. This allows us to confirm both the perfect coherent effect and the size dependence. The schematic structure of the LC network model is shown in Fig.5. The whole computation domain contains 25 layers along the radius, and 30 unit cells in the angular direction for each layer. The blue and the black points in Fig.5(a) represent the MENZ and the double positive material (DPM with positive

permittivity and permeability) regions, respectively. The computational domain is surrounded by Bloch impedances marked by red points, which simulate the matching boundary condition. The equivalent circuit of the unit cells are illustrated in Fig.5(b) and (c). The effective permittivity and permeability of these cells are expressed as ε_R, μ_R, ε_L, μ_L. Here, the subscript "R" and "L" represent DPM and MENZ metamaterials, respectively. The series impedance and the shunt admittance of the MENZ unit cell can be given by

$$Z(\omega) = \frac{1}{j\omega C_L} + \frac{1}{2} j\omega L \qquad (3)$$

$$Y(\omega) = \frac{1}{j\omega L_L} + j\omega C_R . \qquad (4)$$

In our design $\varepsilon_R = \varepsilon_0$, $\mu_R = \mu_0$, $\varepsilon_L \approx 0$, $\mu_L \approx 0$. Given the analogy between Maxwell equations and the transmission line equation, to satisfy these design requirements the equivalent circuit parameters can be derived as $L = \mu_0 \Delta$, $C_R = \varepsilon_0 \Delta$, $L_L = 1/(\mathrm{C}_R \omega^2)$, $C_L = 2/(L\omega^2)$. Here, $\Delta = 0.1c_0 / f$ represents the dimension of the unit cell, f refers to the working frequency of the circuit, and c_0 is the propagation velocity of electromagnetic wave in free space. At the frequency of $f = 510MHz$, parameters for all the elements can be obtained as $L = 72nH$, $C_R = 0.5pF$, $L_L = 180nH$, $C_L = 2.7pF$. The Bloch impedance is $Z_B = 390\Omega$.

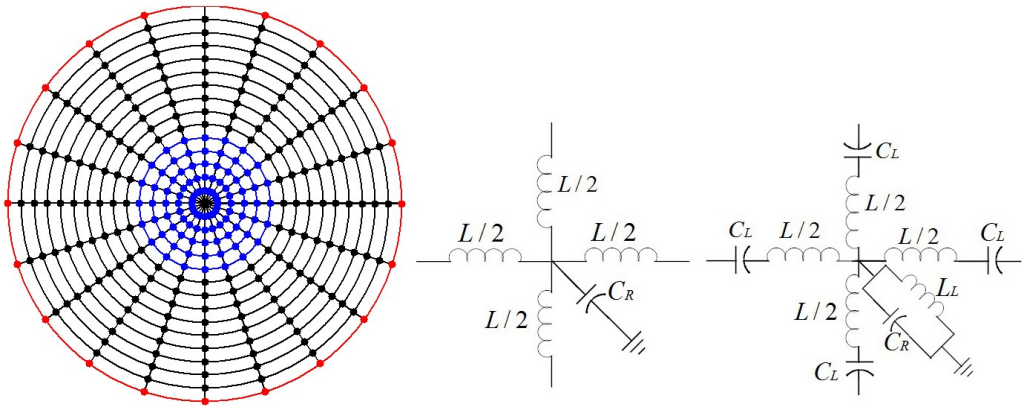

Fig.5. (a) Schematic structure of the LC network model. (b) Unit cell of the DPM region. (c) Unit cell of the MENZ region.

We carry out the simulation using Agilent's Advanced Design System (ADS) circuit simulator. In the simulation, two identical point sources are set separately at two nodes in the MENZ region formed by five layers of unit cells. The voltage is extracted from each node, and the results are plotted in Fig. 6(a). It is seen that the voltage distribution of the two in-phase point sources is perfectly homogeneous as expected, revealing the perfect coherent effect of the MENZ metamaterials. As a comparison, we simulated the voltage distribution pattern of two point sources irradiating in a fully DPM transmission line media, as shown in Fig. 6(b). To investigate the influence of MENZ region size on the irradiation field intensity, we diminish the region from five layers to two layers, and then extract the voltage along the circle which possesses the maximum voltage. The simulation results are shown in Fig. 6(c). Again, the voltage increases with decreasing size, which confirms the previous FEM simulations and the discussion of this behaviour which we provided earlier.

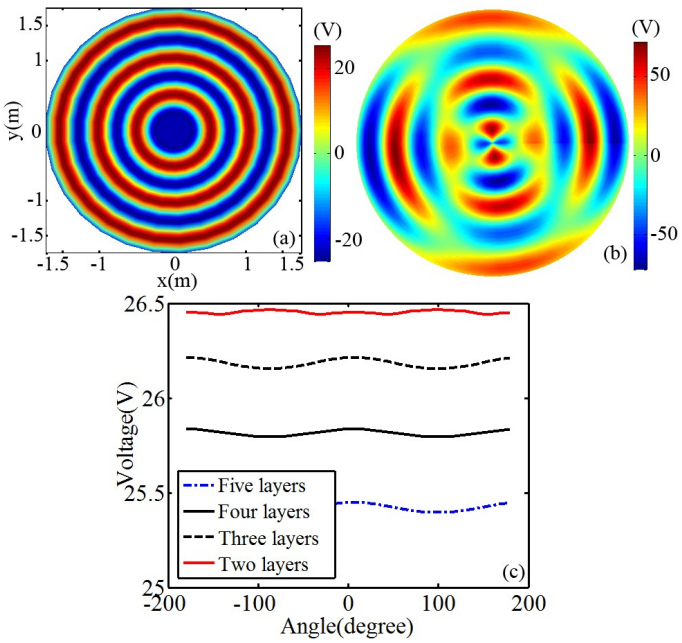

Fig.6. Voltage distribution of the LC network model. (a) The perfect coherent effect for two point sources in a MENZ region and (b) the wave interference phenomenon which is observed in a DPM material. (c) Voltage distribution for the simulation model with different MENZ cell layers.

3. Conclusion

We have demonstrated that MENZ metamaterials can be used for the realization of perfectly coherent effects between multiple in phase sources. The power intensity scales as the square of the number of sources and the resulting radiation pattern is isotropic and arises from the constructive interference of all the sources embedded in the MENZ region. Furthermore it is seen that the geometry of the MENZ metamaterials can enable wavefront tailoring allowing the formation of collimated beams with similar enhanced power. Importantly, we show that the performance of the device is strongly dependent on the size of the MENZ region as the geometric impedance can dramatically increase when the size becomes comparable or larger than the operating wavelength. These effects are also confirmed by L-C network transmission media. Our results provide crucial design guidelines for emerging antennas based on metamaterial concepts. Additionally, they may have potential applications in fields where high power coherent emission is required, such as laser, radar and antenna technologies.

Acknowledgement

This work was supported by the National Natural Science Foundation of China (Grant Nos. 61161007, 61261002), Scientific Research Fund Major Project of the Education Bureau of Yunnan Province (Grant No. ZD2011003), the Specialized Research Fund for the Doctoral Program of Higher Education (Grant No. 20135301110003, 20125301120009), the Natural Science Foundation of Yunnan Province (Grant No. 2011FB018), China Postdoctoral Science Foundation (Grant No. 2013M531989), and the Key Program of Natural Science of Yunnan Province (Grant No. 2013FA006). Y.F. and S.M. acknowledge support from the UK Engineering and Physical Sciences Research Council (EPSRC).